Asian Journal of Chemistry; Vol. 38, No. 2 (2026), 531-542
ASIAN JOURNAL OF CHEMISTRY
https://doi.org/10.14233/ajchem.2026.35099

Sunlight/Visible Light Assisted Photocatalytic Degradation of Acid Alizarin Violet N Dye and 4-Chloro Phenol over M^{n+} Doped Nano TiO_2 Catalysts

BURRI VIJAYALAXMI[1], MYADAM VIJAYATHA[1], SAJEEDA MOHAMMAD[1], NAPPUNNI ROHITHA CHOZHIDYATH[2] and AYTAM HARI PADMASRI[1,*]

[1]Department of Chemistry, University College of Science, Osmania University, Hyderabad-500007, India
[2]Catalysis & Fine Chemicals Department, CSIR-Indian Institute of Chemical Technology, Hyderabad-500007, India

*Corresponding author: E-mail: ahpadmasri@gmail.com; ahpadmasri@osmania.ac.in

Received: 19 October 2025 *Accepted*: 17 January 2026 *Published online*: 31 January 2026 AJC-22272

Nano TiO_2 and 5 wt.% M^{n+} (M = Ag^+, Bi^{3+} and Ni^{2+}) doped nano TiO_2 photo catalysts were synthesised by sol-gel method. The resulting catalysts have been characterised by XRD, UV-Vis DRS, PL, SEM-EDAX, TEM, BET-SA, XPS and Raman spectroscopy. The present research work focused on enhanced photocatalytic degradation of aqueous solutions of acid alizarin violet N (AAVN) dye and 4-chlorophenol (4-CP) were investigated with TiO_2, 5 wt.% Ag/TiO_2, 5 wt.% Bi/TiO_2 and 5 wt.% Ni/TiO_2 nano photocatalysts under visible and solar light. AAVN dye was degraded to an extent of more than 98%, 4-CP degraded 97% on Ag/TiO_2 as compared to Bi/TiO_2, Ni/TiO_2 and Bare TiO_2 nanoparticles. Recyclability of photocatalysts were studied, with the material being found to be stable up to five cycles. Effect of scavengers on the photocatalytic activity of catalysts was studied using both superoxide ion radical and hydroxyl ion radical/hole scavengers namely benzoquinone, isopropanol, ammonium oxalate and formic acid, respectively.

Keywords: Acid Alizarin Violet N, 4-Chlorophenol, Photo degradation, Doped TiO_2.

INTRODUCTION

Dyes are extensively used in a wide range of technological and industrial applications, particularly in various sectors of the textile industries [1,2] and the leather tanning industry [3,4]. In addition, dyes find widespread use in paper manufacturing, agricultural research, food technology, hair dyeing, and light-harvesting systems. Acid Alizarin is a commonly employed dye and has also been used as an organic marker [5]; however, many dye-stuffs are classified as priority and hazardous pollutants due to their persistence and toxicity in wastewater. The uncontrolled discharge of dye-containing effluents poses significant environmental and health concerns, necessitating the development of effective remediation strategies [6,7].

Among the various approaches explored for pollutant removal, photocatalytic degradation has emerged as a promising and environmentally benign technique. Titanium dioxide (TiO_2) is one of the most extensively studied photocatalysts for the degradation of both inorganic and organic pollutants owing to its low cost, high chemical stability, low toxicity, and strong oxidative capability [4]. Despite these advantages, the wide band gap of TiO_2 restricts its activity primarily to the ultraviolet region, which limits its efficiency under visible light. Consequently, considerable research efforts have been directed toward developing modified TiO_2-based photocatalysts that exhibit enhanced activity and stability under visible light irradiation.

Doping TiO_2 with selective metal ions has been demonstrated as an effective strategy to reduce its band gap and extend its photoresponse into the visible region [8-11]. The incorporation of metallic elements can introduce additional energy levels within the band structure of TiO_2, thereby improving light absorption and suppressing the recombination of photogenerated electron-hole pairs. Transition metals such as Ni, Cr, Zn and noble metals like Ag, as well as post-transition metals including Bi, have shown considerable potential in enhancing photocatalytic performance [12-15]. Doping with these metals not only improves photon absorption but also facilitates efficient charge separation, leading to improved photocatalytic activity [16-18].

Among these dopants, Ag-doped TiO_2 has been widely reported as an efficient photocatalyst for the degradation of

various organic contaminants. The presence of an optimal amount of Ag enhances visible light absorption and reduces the effective band gap of TiO_2, thereby promoting photocatalytic efficiency [17]. Similarly, Bi-based nanomaterials have attracted significant attention due to their low cost, high stability, non-toxicity, and strong photoactivity. Bi- and Ag-doped TiO_2 systems have been reported to exhibit superior visible-light driven photocatalytic performance for the degradation of organic pollutants, attributed to their excellent light absorption properties and effective charge carrier separation [13-15]. The introduction of Bi-related energy levels below the conduction band of TiO_2 further contributes to band gap narrowing and enhanced visible light absorption, making such doped systems highly promising for wastewater treatment applications. The present work is aimed at the synthesis of TiO_2 NP, Ag/TiO_2, Bi/TiO_2 and Ni/TiO_2 by sol-gel method and for its application in AAVN dye decolourisation and 4-chlorophenol (4-CP) degradation.

EXPERIMENTAL

Titanium tetraisopropoxide (TTIP, NR chem), silver nitrate ($AgNO_3$; 99%), bismuth nitrate pentahydrate ($Bi(NO_3)_3 \cdot 5H_2O$; 98%), nickel nitrate hexahydrate ($Ni(NO_3)_2 \cdot 6H_2O$: 98% SD Fine Chemicals), ethanol, isopropyl alcohol (Moly Chem), glacial acetic acid (Merck) were used without further purification for the preparation of catalysts.

Synthesis of Ag/TiO_2, Bi/TiO_2, Ni/TiO_2 and bare TiO_2 nano-photocatalysts: A 5 wt.% Ag doped nano-TiO_2 was prepared by acid modified sol-gel method. Initially, 5 wt.% of $AgNO_3$ was dissolved in 120 mL of deionised water at room temperature, followed by addition of 10 mL of glacial acetic acid. In the next step, 28 mL of titanium tetraisopropoxide was dispersed in 80 mL of absolute ethanol with continuous stirring. Then the above two solutions were added dropwise together within 2 h under continuous stirring. Afterwards, the attained sol was stirred incessantly for 3 h and dried for 3 days at room temperature. As synthesised TiO_2 gels were dried at 80 ºC for 12 h. The resultant solids were powdered and calcined at 500 ºC for 4 h. Undoped TiO_2, Ni/TiO_2 [19] and Bi/TiO_2 nanoparticles were prepared using same above sol-gel method for comparative studies using bismuth nitrate hexahydrate and nickel nitrate hexahydrate as precursors of Bi and Ni. The prepared Ag doped TiO_2, Bi doped TiO_2 and Ni doped TiO_2 denoted as AgT, BiT and NiT nanocatalysts.

Characterisation: The Rigaku miniplex diffractometer was used to observe powder X-ray diffraction (XRD) patterns while using a Cu*K*α (1.5406 Å) radiation source at 40 V and 15 mA. The morphology and particle size were characterised by transmission electron microscope (TEM, model JEOL 1010) instrument, operating at 100 kV with a field emission gun. The surface properties of fresh catalysts were measured by N_2 adsorption at -196 ºC (Micrometric ASAP 2010 surface analyzer). The BET method was employed to determine specific surface area. X-ray photoelectron spectroscopy (XPS) was employed to investigate the oxidation states of the doped metal ions and their interactions within the TiO_2 lattice. The KRATOS-AXIS 165 with dual aluminum–magnesium anodes was used to record Mg*K*α radiation. The X-ray power supply was run at 15 kV and 5 mA. Raman spectral data captured using He-Ne laser emitted at 633 nm line scattered light was examined by using HORIBA JOBIN YVON HR800, Japan. The laser was focused at ~3 μm and backscattered Raman signal was collected using a 10X lens. UV-Vis diffuse reflectance spectra (DRS) were recorded using JASCO V650 UV-Vis spectrophotometer in region of 200-800 nm. JASCO FP-8500 spectrofluorometer used in the present research work recorded photoluminescence spectra (PL) at room temperature with an excitation wavelength of 220 nm.

Photocatalytic degradation of acid alizarin violet N (AAVN) dye and 4-chlorophenol (4-CP): The photocatalytic degradation of pure TiO_2 NP, AgT, BiT and NiT was determined by the degradation AAVN and 4-CP under solar and visible light irradiation. The photocatalytic studies were carried out on a reactor supplied by Lelesil innovative system; India equipped with 250 W visible lamp. In a typical process, 50-150 mg of catalysts was added to 50-200 ppm AAVN dye/4-CP solution and dispersed before irradiation by visible and sunlight with stirring. The mixture was agitated for a duration of 60 min in directive to establish adsorption-desorption equilibrium. The catalyst was filtered and absorption spectra of the attained aliquot were measured using Ultra Violet-Visible spectrophotometer to monitor the degradation of AAVN dye and 4-CP from time to time. The degradation rate was calculated using the following equation:

$$\text{Degradation rate } (\%) = \frac{C_o - C}{C_o} \times 100 \quad (1)$$

RESULTS AND DISCUSSION

Powder X-ray diffraction analysis: To study the crystal structure of bare TiO_2, NiT, BiT and AgT nanocatalysts calcined at 500 ºC, XRD investigation was carried out in the range of $2\theta = 10\text{-}80^\circ$. The doping of Ag, Ni or Bi in TiO_2 lattice did not alter anatase phase diffraction patterns (Fig. 1). In case sol-gel synthesised catalysts AgT, NiT, BiT and neat TiO_2

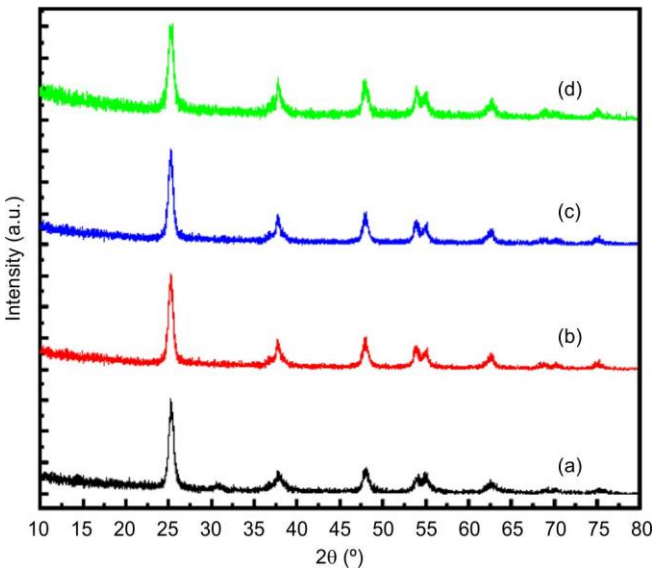

Fig. 1. XRD patterns of (a) bare TiO_2 (b) AgT (c) NiT and (d) BiT nano photocatalysts

TABLE-1
STRUCTURAL AND MORPHOLOGICAL DATA OF TIO_2 AND ITS DOPED NANOCATALYSTS

Catalyst	*d*-spacing (Å)	Lattice parameters (Å)		Volume $(Å)^3$	Surface area (m^2/g)	Average crystallite size (nm) from XRD	Average particle size (nm) from TEM
		a = b	c				
TiO_2	3.517	3.786	9.500	136.17	57	11.18	8.25
AgT	3.525	3.789	9.606	137.91	60	8.85	7.75
NiT	3.515	3.787	9.458	135.64	54	10.03	8.00
BiT	3.525	3.789	9.606	137.91	92	7.24	7.85

showed XRD pattern with, foremost diffraction peaks at 2θ = 25.3º, 37.7º, 48.03º, 53.97º, 55.13º, 62.52º, 68.82º, 70.14º and 75.22º. These diffraction peaks (2θ) correspond to Bragg's reflection planes (101), (004), (200), (105), (211), (204), (116), (220) and (215), respectively. Parent TiO_2 and NiT, BiT and AgT show pure anatase phase with tetragonal structure consistent with JCPDS data (card no 21-1272) [20,21]. The parent TiO_2 showed traces of brookite phase at 2θ = 30.81º (JCPDS card 29-1360) corresponding to (121) plane.

Using Scherrer's formula (eqn. 2), the average crystallite size of pure TiO_2, AgT, NiT and BiT from prominent peaks in the XRD was calculated.

$$D = \frac{K\lambda}{\beta_{hkl}\cos\theta} \quad (2)$$

where D is the average crystallite size; λ is the wavelength of radiation and β is the FWHM (full width at half maximum); θ is the Bragg angle; and K is the Scherer's constant. The crystallite size of bare TiO_2, AgT, NiT and BiT were found to be 11.18, 8.85, 10.03 and 7.24 nm, respectively. The lattice parameters 'a = b', 'c' and unit cell volume 'V' were calculated from the peaks of (101) and (200) of anatase using the Bragg's equation:

$$a = \frac{\lambda}{\sqrt{3}\sin\theta}\sqrt{(h^2 + hk + k^2)} \quad (3)$$

$$c = \frac{\lambda}{2\sin\theta}l \quad (4)$$

$$V = a^2c \quad (5)$$

for TiO_2 and doped TiO_2 nanoparticles. The slight expansion of the unit cell upon Ag and Bi doping can be attributed to the incorporation of larger dopant ions into the TiO_2 lattice (Table-1).

SEM-EDAX: The SEM and EDAX micrographs of bare TiO_2, AgT, NiT and BiT nanophotocatalysts are displayed in Fig. 2a-d, respectively. It can be clearly seen that the shapes of synthesised nanoparticles are spherical with minimal agglomeration as compared with bare TiO_2 nanoparticles [22,23]. The surface morphology of Ag-, Bi- and Ni-doped TiO_2 appears smooth and uniform. The atomic ratios of Ag in Ag-doped TiO_2, as well as those of Ni in Ni-doped TiO_2, along with Ti and O, are presented in Fig. 2. The presence of distinct signals corresponding to Ag, Bi, and Ni, in addition to the main constituents Ti and O, confirms the successful incorporation of these dopant elements into the TiO_2 host lattice rather than their segregation as separate phases.

TEM and SAED: TEM analysis also reveals the spherical morphology of bare TiO_2 and AgT nanoparticles. The TEM observations are consistent with the average crystallite size estimated from the XRD patterns. The particle size distribution histograms shown in Fig. 3e-f further confirm the relatively uniform size distribution of the synthesized particles. The selected area electron diffraction (SAED) patterns presented in Fig. 3c-d exhibit well-defined concentric rings with distinct diffraction spots, indicating the crystalline nature of the catalysts. The presence of such ring patterns is characteristic of polycrystalline TiO_2, confirming that the catalysts consist of multiple crystalline domains.

UV-Vis DRS and photoluminescence analysis: The absorption edge of TiO_2 below 370 nm is generally attributed to charge transfer from the valence band to the conduction band. A red shift in the absorption edge toward longer wavelengths indicates a reduction in band gap energy, which enhances visible light absorption, suppresses electron-hole recombination and consequently improves photocatalytic activity. Using absorption edge wavelengths from inset graph Fig. 4a band gap energy values of bare TiO_2, AgT, NiT and BiT were calculated and shown in Table-2. The band gap energy (E_g) was determined by using eqn. 6:

$$E_g = \frac{1239.8}{\lambda} \quad (6)$$

where λ is the wavelength (nm) of the absorption edge in the spectrum. Using above equation and Kubelka-Munk plot calculated band gap energies of photocatalysts. Metal ion doping resulted in lowering of band gap than parent TiO_2, shift in absorption wavelength to visible region and hence enhanced photocatalytic degradation of dye/organic pollutant.

TABLE-2
OPTICAL CHARACTERISTIC DATA OF THE NANOPHOTOCATALYSTS

Catalyst	Absorption wavelength edge (nm)	Band gap energy (eV)	Emission wavelength (nm)
TiO_2	397	3.12	401
AgT	478	2.59	420
NiT	464	2.67	412
BiT	437	2.83	407

Photoluminescence spectra Fig. 4b of bare TiO_2, Ag, Ni and Bi doped TiO_2 nanoparticles at an excitation wavelength of 360 nm for exciting all these catalysts displayed one peak around UV region and other three peaks at near visible region due to metal ion doping indicated by the broadening in optical emission band, which is related to the columbic interaction effect. Due to the charge transfer from Ti^{3+} to oxygen the blue-green emission bands appeared at 401, 420 and 412 nm [24]. This indicates the origin of bands from the intrinsic state

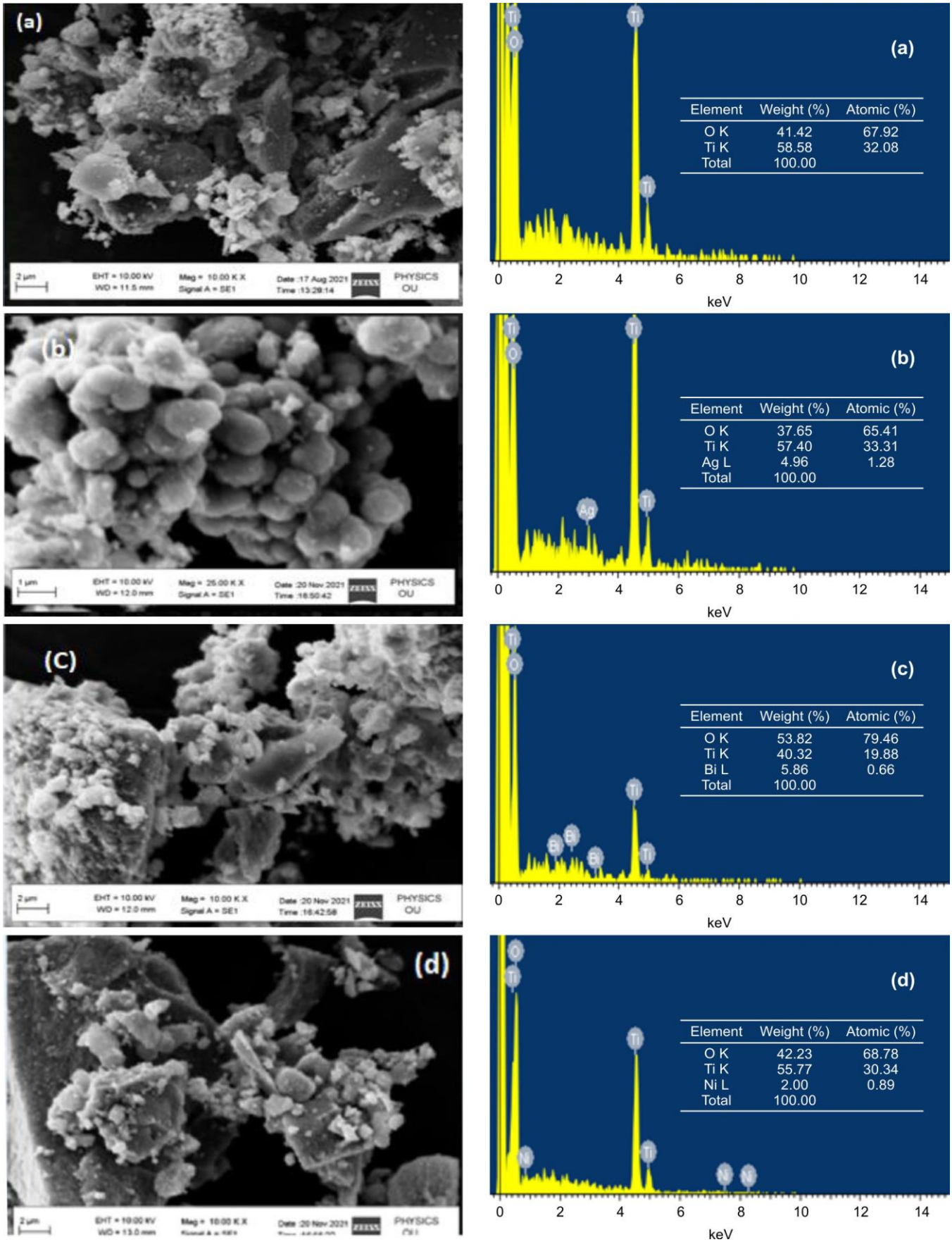

Fig. 2. SEM images and EDAX patterns of (a) TiO_2 (b) AgT (c) BiT and (d) NiT NPs

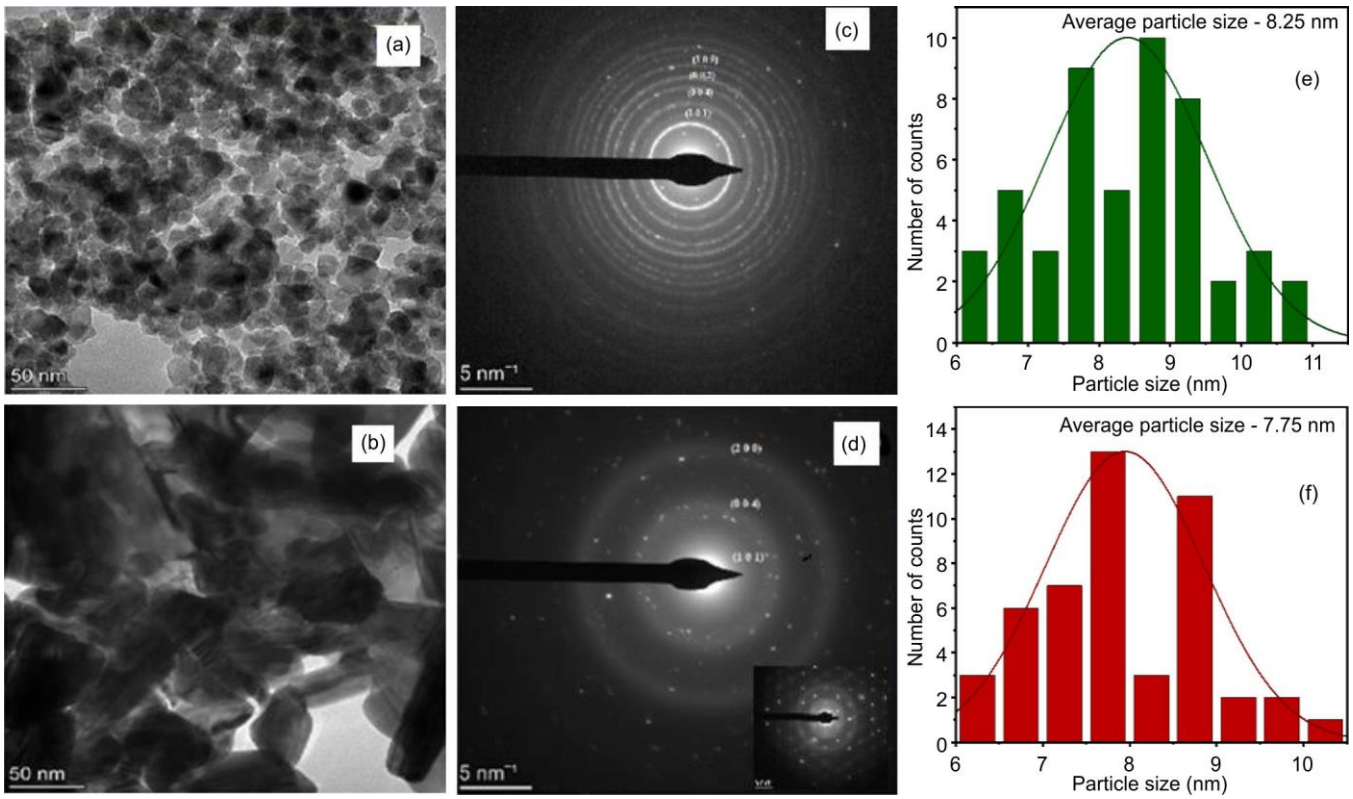

Fig. 3. Transmission electron microscope images of (a)TiO_2 and (b) AgT, SAED images of (c)TiO_2 and (d) AgT and histograms of (e) TiO_2 and (f) AgT

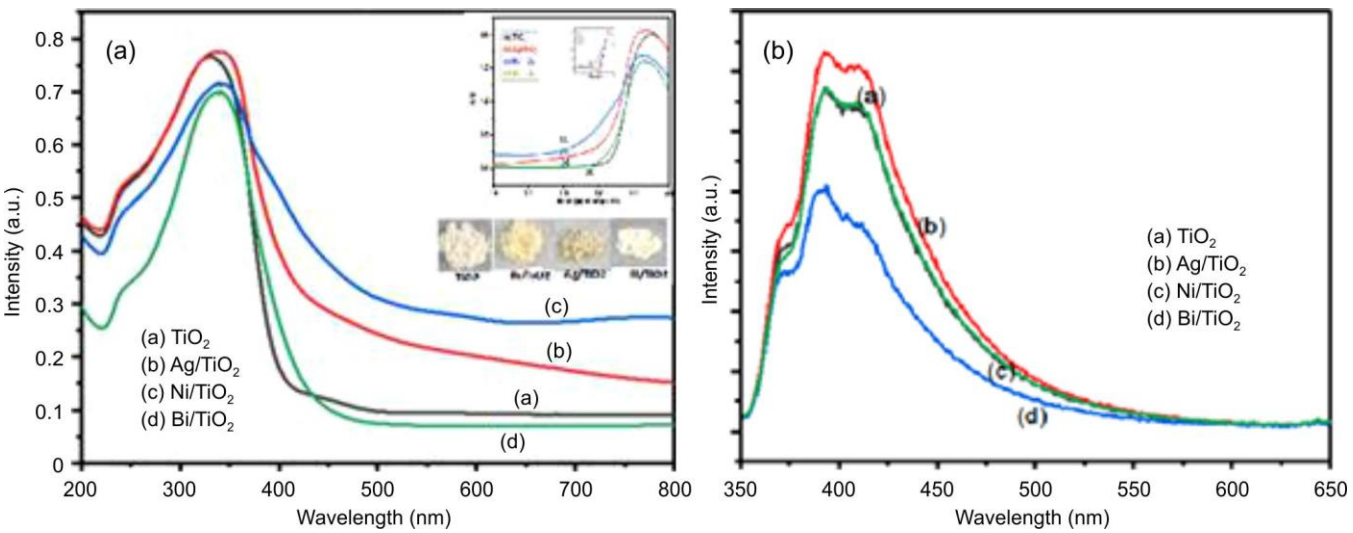

Fig. 4. (a) Ultra violet-visible DRS and (b) photoluminescence spectra of cation doped TiO_2 nanocatalysts

rather than the surface state. These luminescence peaks are attributed to the bulk defects in the modified TiO_2 nanoparticles. AgT, BiT and NiT nanocatalysts showed a red shift due to vacancy of Ti and O, Ni and Bi ions well dispersed in TiO_2, hence emission intensity decreases. The oxygen vacancies and defects are responsible for the photoluminescence emissions of semiconductor oxides like TiO_2. However, in case of doped TiO_2, the surface oxygen vacancies capture the electrons and the metal ions capture the holes and reduce the recombination rate of electron-hole pairs. Also, the new defect levels created by the dopant ions near the conduction band minimum are occupied by the excited electrons from valence band further are responsible for the lowering of the PL intensity [25].

BET-Surface area measurements: The specific surface area and pore structure of synthesised nanoparticles were examined by performing N_2 adsorption-desorption measurements. All the adsorption isotherms were type-IV class as per the IUPAC nomenclature. BET surface areas of AgT and BiT nanoparticles showed higher specific surface areas than bare TiO_2 and these values are shown in Table-1.

XPS results: X-ray photoelectron spectra (XPS) of the catalysts were analysed for surface elemental composition and

valence states of elements in bare TiO_2, BiT, AgT and NiT (a wide scan shown in Fig. 5). The characteristic peaks of Ti 2p, O 1s, Ni 2p, Ag 3d and Bi 4*f* of the photocatalysts are displayed in Fig. 6. The observed peaks at 458.5 and 464.5 eV for Ti represent the spin-orbital splitting of Ti $2p_{3/2}$ and Ti $2p_{1/2}$, respectively indicating a state of Ti^{4+} in sample. It can be confirmed that Ti at the surface exist in the form of Ti^{4+}, which can transform to Ti^{3+} by trapping photogenerated electrons [26]. O 1s peak at 530 eV can be linked to oxygen bound to Ti^{4+} in TiO_2 and is found to be shifted to lower energies with the addition of the doped cation in the order of $Bi^{3+} > Ag^{+} > Ni^{2+}$ attributed by Yu *et al.* [26]. as to the differences in their electronegativity with Ti. This peak is accompanied by a shoulder at 532 eV that can be observed upon deconvolution (not shown in the figure), which was attributed to the adsorption of OH group on the surface that can produce surface bound OH radicals on reaction with photo induced holes responsible for high oxidation reactivity [27].

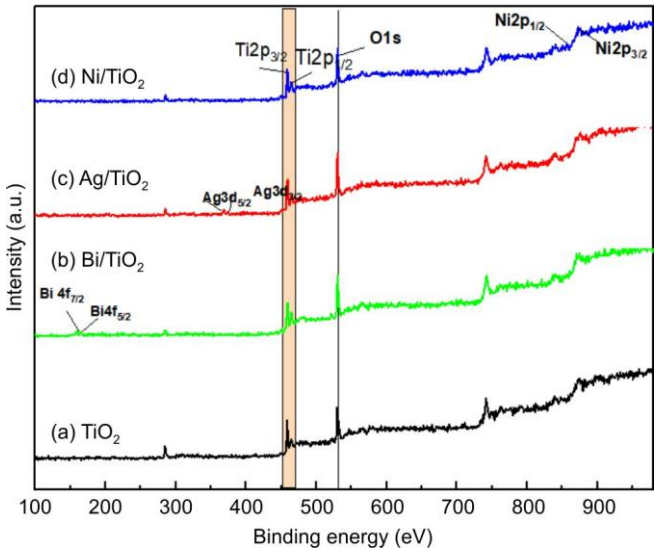

Fig. 5. Wide scan XPS spectra of TiO_2 based nanocatalysts

Fig. 6c illustrate the split of the 3*d* peak into two distinct peaks at 373 eV and 367.6 eV, corresponding to Ag $3d_{3/2}$ and Ag $3d_{5/2}$, respectively. The XPS line for Bi 4*f* shown in Fig. 6e display two distinct peaks at 164.6 and 159 eV, signifying the binding energies of Bi $4f_{7/2}$ and Bi $4f_{5/2}$, respectively. This observation suggests the presence of Bi in the sample is in its +3 oxidation state. The binding energies at 856 and 873.1 eV for Ni $2p_{1/2}$ and Ni $2p_{3/2}$ are attributed to the splitting of Ni 2*p*. Shoulder peaks just besides these main peaks of Ni 2*p* are indicative of presence of satellite peaks corresponding to the Ni^{2+} [28].

Raman spectroscopy: Raman spectra of the as-prepared TiO_2, AgT, NiT and BiT nanocatalysts are shown in Fig. 7. The four peaks shown by each catalyst are due to the anatase phase identified at values of 144, 396, 514 and 639 cm^{-1} of TiO_2, 144.6, 395.6, 514.7 and 638.4 cm^{-1} of Ag/TiO_2, 145, 394.2, 515.4 and 637.6 cm^{-1} of Bi/TiO_2 and 144.1, 399, 516.3 and 637 cm^{-1} of Ni/TiO_2. The peaks located at 144 and 639 cm^{-1} (E_g) correspond to Ti-O stretching mode, the peak at 515 cm^{-1} ($A_{1g} + B_{1g}$) refers to the stretching mode of Ti-O peak, at 397 cm^{-1} (E_g) allocated to the O-Ti-O bending mode [26]. A shift in the E_g mode at 144 cm^{-1} of TiO_2 to higher values with doping and a broadening of this peak is suggestive of decreased particle size that correlate well with TEM and XRD data.

Photocatalytic activity of AAVN dye: The optical density of AAVN solution was measured at 546 nm with a UV-Visible spectrophotometer. The efficiency of photocatalytic decomposition of dye was calculated; the % degradation of dye as against time of irradiation from this study implied an increase in % degradation with time. The degradation of 100 ppm AAVN dye degradation achieved nearly was 95%, 98%, 96.7% and 96% using 75 mg of bare TiO_2, 5 wt.% AgT, 5 wt.% BiT and 5 wt.% NiT NP under visible light irradiation, respectively. Also, the doped catalysts and parent TiO_2 showed 60-90% degradation of 150 ppm of AAVN dye. Even at high concentration *i.e.*, 200 ppm AAVN dye decomposition achieved nearly was 72%, 87.8%, 74.4% and 73% using 75 mg of bare TiO_2, 5 wt.% AgT, 5 wt.% BiT and 5 wt.% NiT, respectively. The steady-state degradation of dye solution was observed nearly at 180 min of time. The order of degradation efficiency of doped and undoped catalyst is:

$$AgT > BiT > NiT > TiO_2$$

A maximum degradation efficiency of 98% was achieved for the 100 ppm AAVN dye solution using 75 mg of AgT photocatalyst, which was significantly higher than that obtained with NiT, BiT and undoped TiO_2 (Fig. 8).

In sunlight AAVN dye photocatalytic activity was evaluated by using 100 mL of 50 ppm (0.05 g L^{-1}) dye solution with 75 mg of bare TiO_2, Ag doped TiO_2, Bi doped TiO_2 and Ni doped TiO_2. The degradation efficiency was found to be higher that is 63% using 5 wt.% BiT nanoparticles with 50 ppm AAVN dye solution than over AgT, NiT and bare TiO_2 (Fig. 8).

The photocatalytic degradation of AAVN dye follows pseudo-first-order kinetics, consistent with the Langmuir-Hinshelwood model. Accordingly, the rate of degradation of AAVN dye can be expressed by the following equation:

$$\ln\left(\frac{C}{C_o}\right) = -kt \qquad (7)$$

In this context r, rate is proportional to the C_t concentration at time t, reactant adsorption constant is K and k is the reaction rate constant. The first order kinetics of AAVN dye degradation is verified by the graph of ln C/C_o *vs.* t in Fig. 9 which is a straight line. The pseudo-first-order rate constants were calculated using eqn. 7 and the results are summarized in Table-3. A relatively good correlation to the first-order reaction kinetics was found as indicated by the regression correlation coefficient (R^2) and the rate of degradation increased with metal ion doping in TiO_2. The AgT exhibited higher photocatalytic activity of AAVN degradation over the rest of the catalysts studied.

Photocatalytic activity of 4-chlorophenol: The % degradation was examined using UV-Vis spectrophotometer at 225 nm. The 75 mg of photocatalyst *viz.*, TiO_2, AgT and BiT was suspended in 50 mL of 4-CP (50 ppm) irradiated under visible light showed 68.2%, 97.1%, 93.4% of degradation, respectively as indicated in Fig. 10. Degradation efficiency of TiO_2,

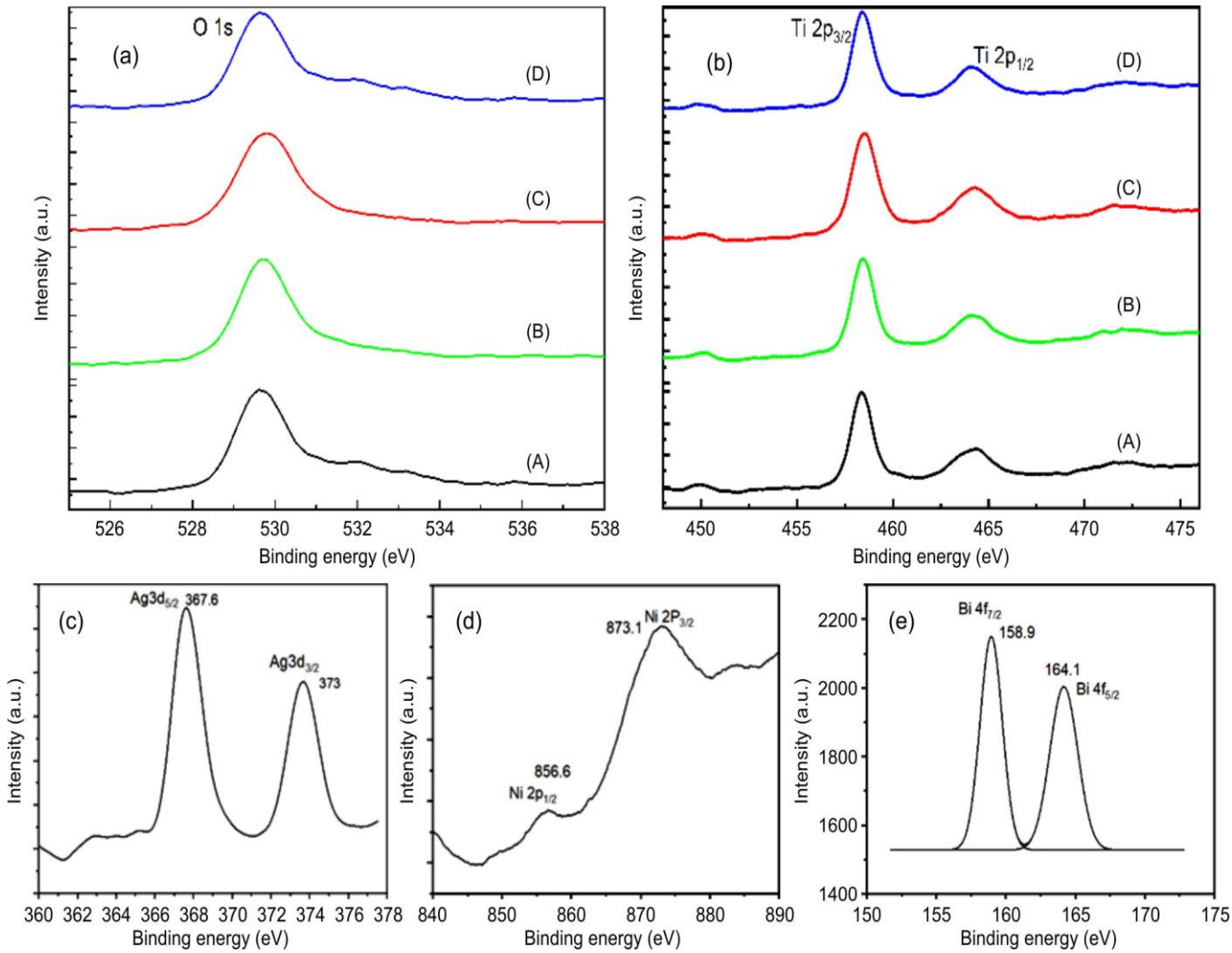

Fig. 6. X-ray photoelectron spectra of (a) O 1s and (b)Ti 2p XPS of (A) TiO_2 (B) AgT (C) BiT and (D) NiT of nanocatalysts; (c) Ag 3d (d) Ni 2p and (e) Bi 4f of the corresponding cation doped TiO_2 photocatalysts

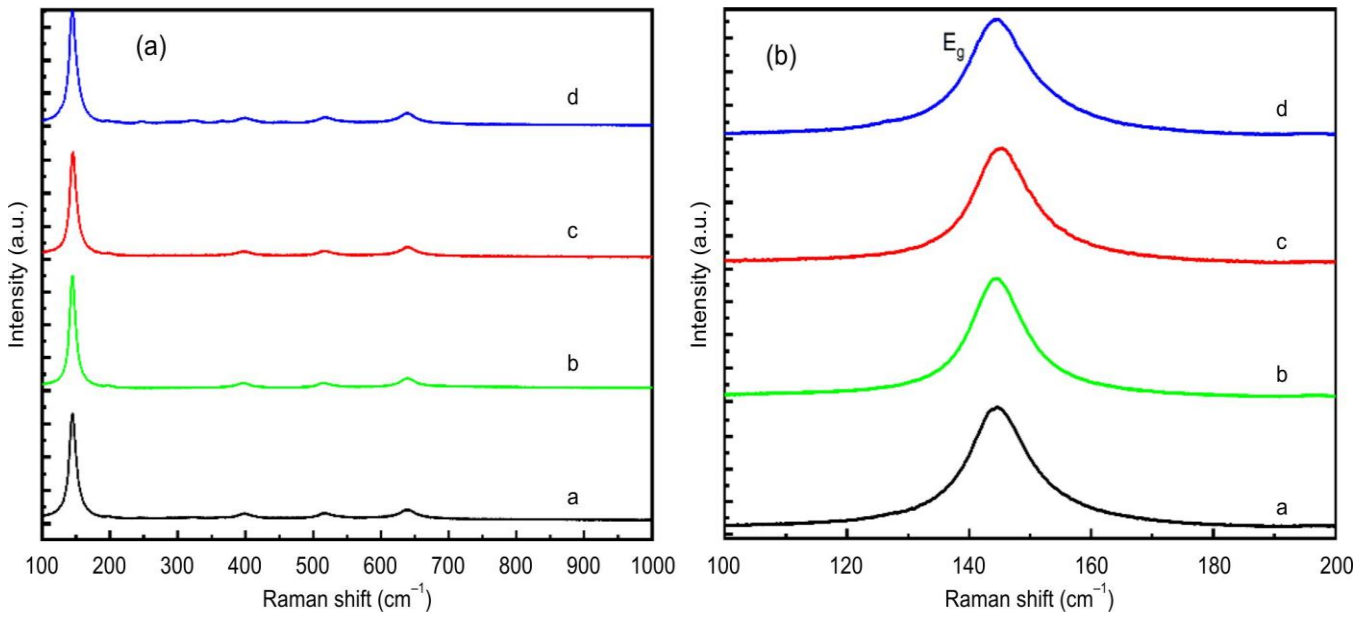

Fig. 7. Raman spectra of (a) TiO_2 (b) AgT (c) BiT and d) NiT nanocatalysts

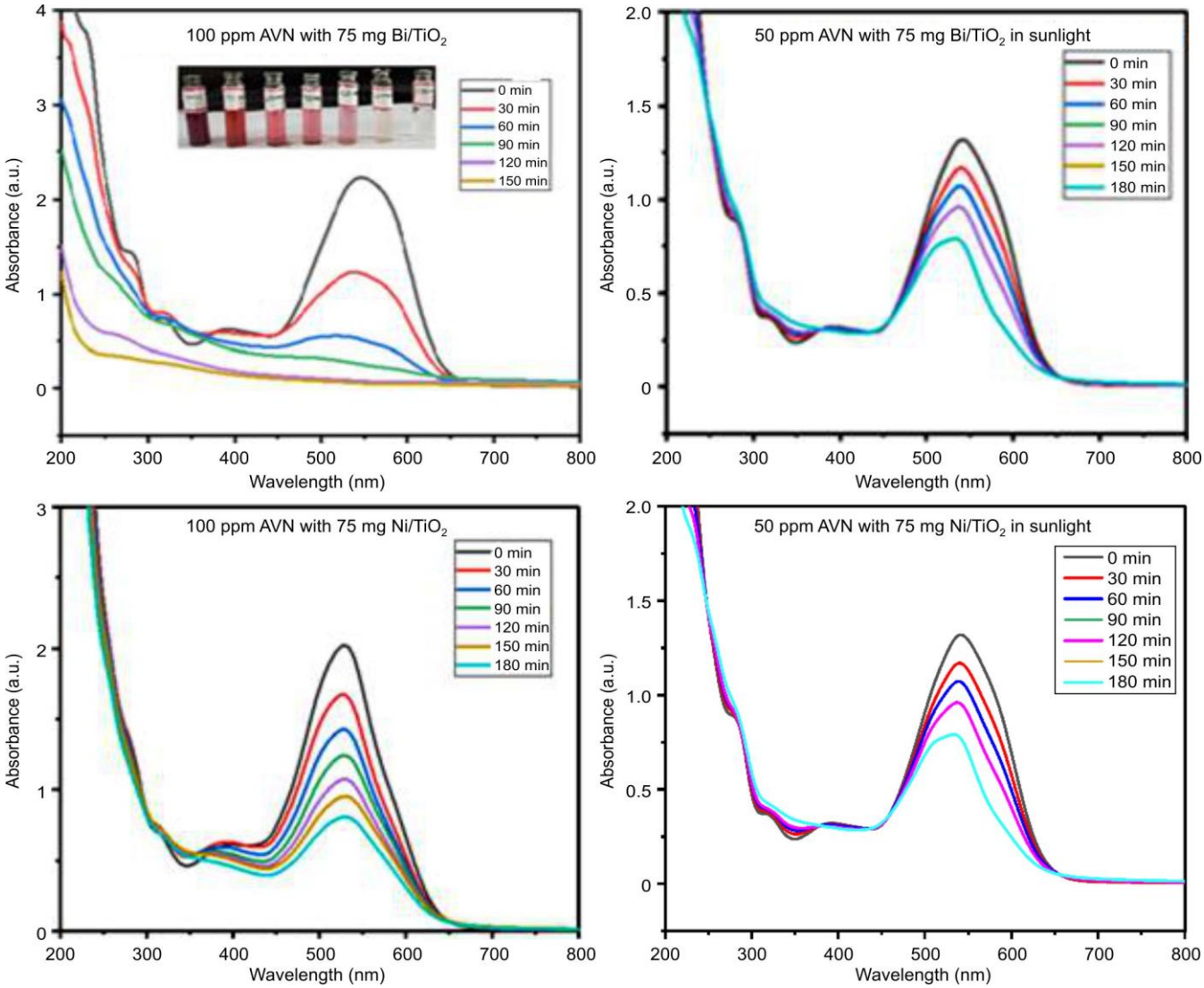

Fig. 8. UV-Visible absorption spectra of BiT, NiT in visible and sunlight

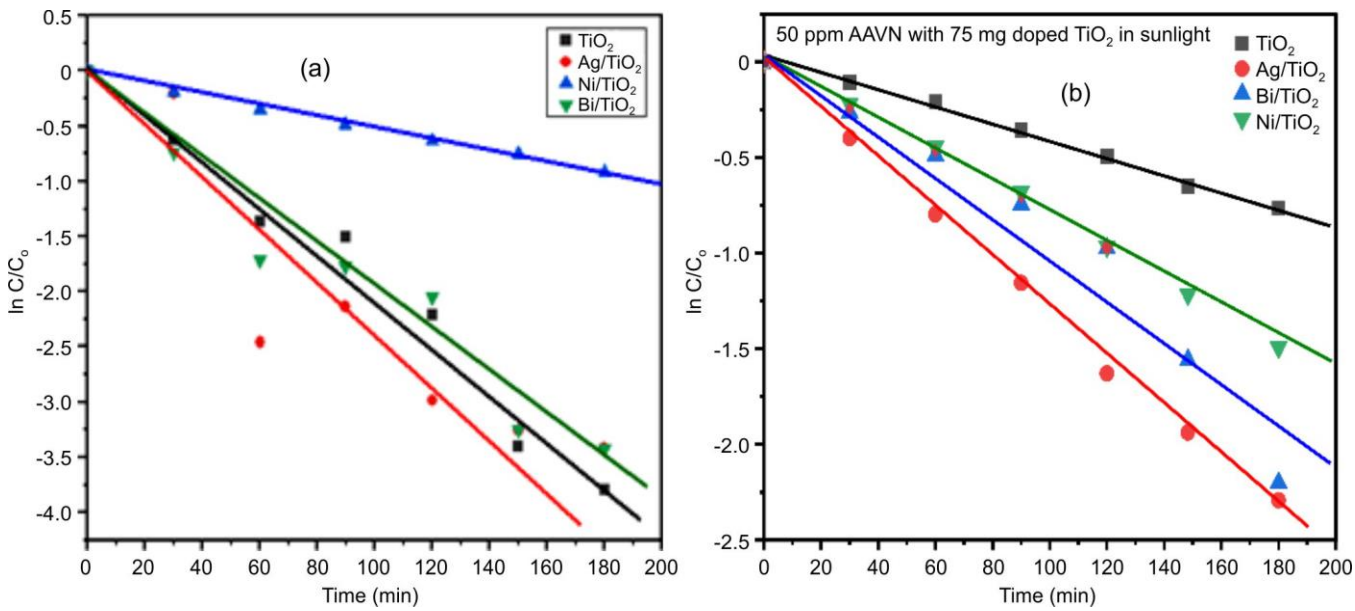

Fig. 9. Plots of ln C/C_o *vs.* time for TiO_2 and cation doped TiO_2 in (a) visible light and (b) sunlight

TABLE-3
RATE CONSTANTS OF AAVN DYE AND 4-CP DEGRADATION OVER TIO_2 AND DOPED TIO_2 NANOCATALYSTS

Catalyst	Rate constant (min^{-1}) of 4-CP in visible light × 10^3	Rate constant (min^{-1}) of AAVN dye in visible light × 10^2	Rate constant (min^{-1}) of 4-CP in sunlight × 10^3	Rate constant (min^{-1}) of AAVN dye in sunlight × 10^2
TiO_2	0.66	0.83	0.24	0.44
AgT	0.23	1.28	1.30	1.20
BiT	0.16	1.15	1.20	1.01
NiT	–	0.93	–	0.84

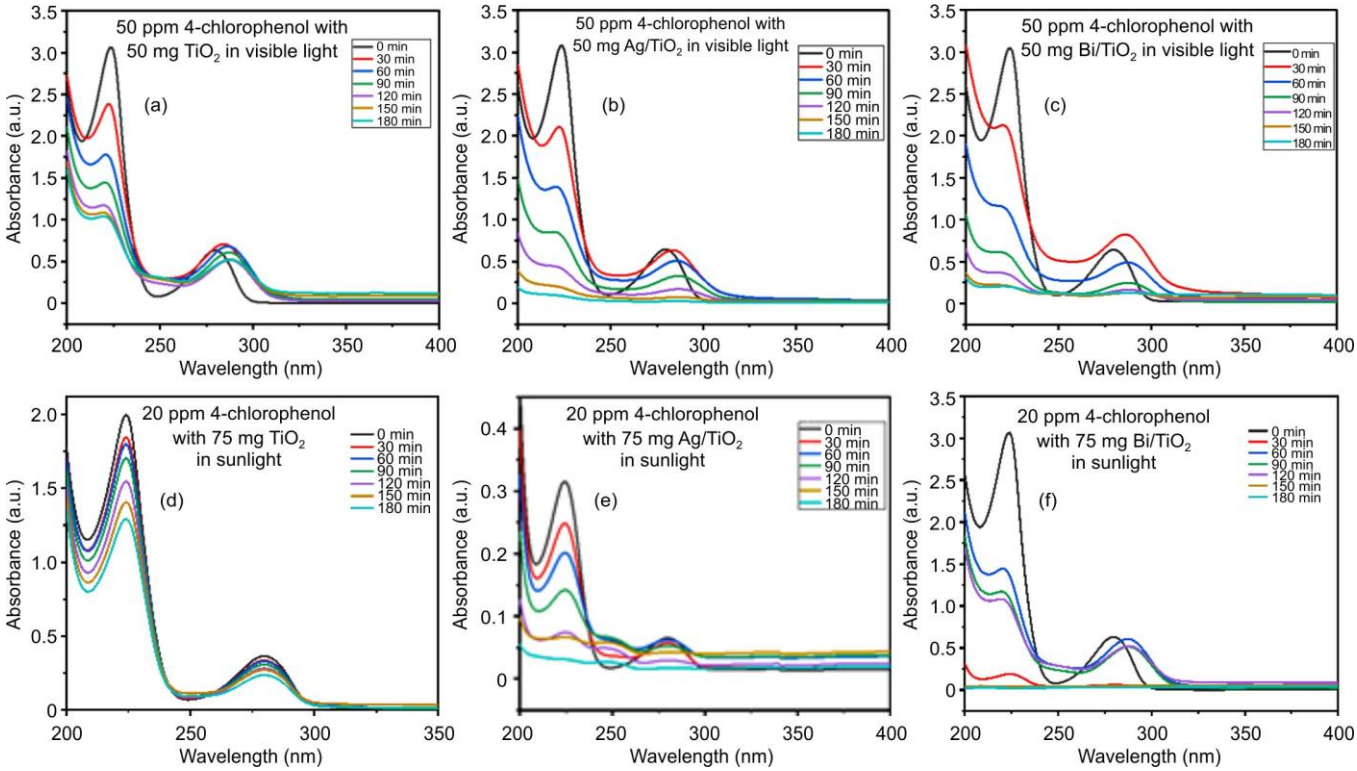

Fig. 10. UV-Vis absorption spectra of (a) TiO_2 (b) AgT and (c) BiT NP in visible and (d) TiO_2 (e) AgT and (f) BiT nanocatalyst in sunlight

AgT and BiT was 35%, 90% and 87% of 4-chlorophenol (20 ppm) under sunlight irradiation, respectively. Doped TiO_2 showed higher degradation compared to bare TiO_2 under visible light and sunlight irradiation.

The graph of ln C/C_0 *vs.* time (Fig. 11) is a straight line, confirming that degradation 4-CP organic pollutant follows a pseudo-first-order kinetics. The activity showed a good fit in the first-order rate equation and the doped TiO_2 catalysts showed

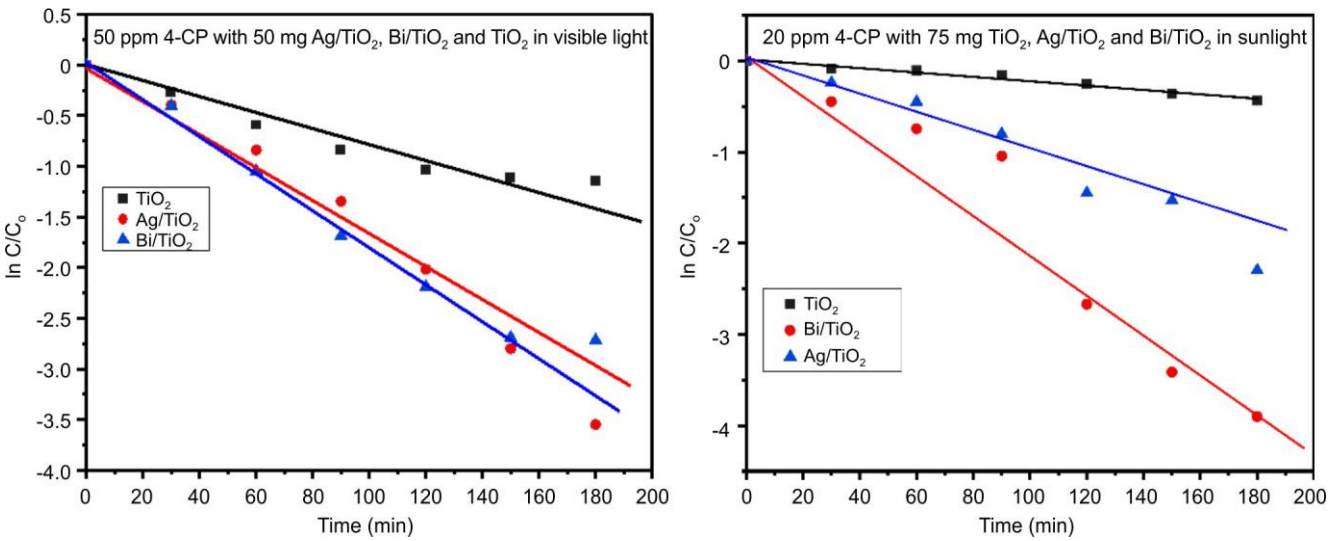

Fig. 11. Plots of ln C/C_o *vs.* time for TiO_2, AgT and BiT nanocatalysts

higher rates of degradation of 4-CP clearly established the promoting effect of the dopant in enhancing the degradation rate of 4-CP. The outstanding photocatalytic activity of the 4-CP organic pollutant could be ascribed to the BiT.

The higher degradation rate of AAVN dye/4-CP in visible/sunlight can be ascribed to the role played by the metal ions whose the redox potentials $E^o(Ag^+/Ag)$, $E^o(Bi^{3+}/Bi)$ and $E^o(Ni^{2+}/Ni)$ are 0.79 V, 0.226 V and -0.25 V, respectively that are in between the conduction band potential E_{CB} (-0.5 V *vs.* NHE) and valence band potential E_{VB} (2.7 V *vs.* NHE) of TiO_2 as described by Yu *et al*. [26]. They attributed it to the photosensitisation process where the electrons from LUMO levels of the dye molecules that move on to the conduction band of TiO_2 being trapped up by the metal ion species and thus contributing to the separation of electron-hole pairs.

Regeneration and scavenger studies: The reusability and stability of the catalysts were established for the decolorisation of AAVN under indistinguishable reaction at ambient conditions. The used photocatalyst was washed with water and dried in a hot air oven before use in the next cycle of photocatalytic reaction. Fig. 12 displays the outcome of AAVN degradation for five cycle runs. AgT, BiT, NiT and bare TiO_2 shows remarkable photo stability as the AAVN degradation activity after fifth cycle were observed as 97%, 90.3%, 69% and 67%, respectively. The degradation efficiency was slow with a slight decrease in each cycle. There was no noteworthy change in the degradation of AgT after completing the 3rd cycle. Only 1% loss in Ag doped TiO_2, 5% loss in Bi-doped TiO_2 and Ni-doped TiO_2, 20% loss in bare TiO_2 activity was observed. The aforementioned results recommend good stability of the photocatalyst, which remains unaffected even after five sequential runs.

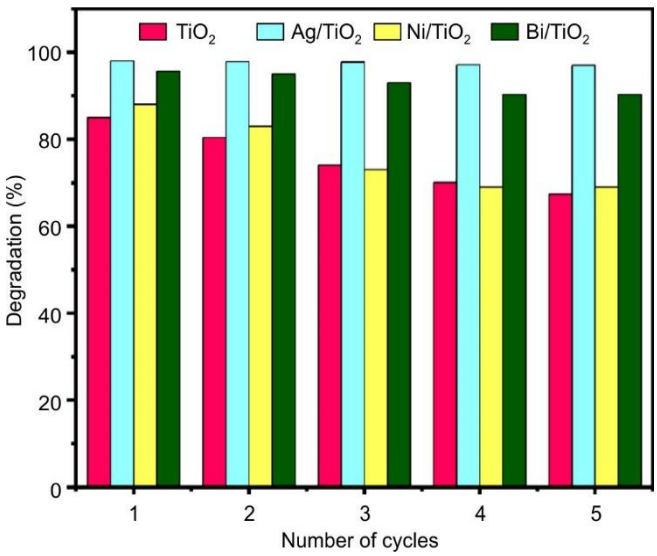

Fig. 12. Reusability data of TiO_2, AgT, BiT and NiT nanocatalysts

Fig. 13 reveals XRD of used and unused AgT nanoparticles. AgT showed higher % degradation compared to BiT, NiT and bare TiO_2 NP. The stability of AgT nanoparticles after fifth cycle of reaction was examined by XRD. The XRD of used catalyst showed no changes when compared to that of unused catalyst indicating an intact structure of the catalyst even after 5 runs of the reaction.

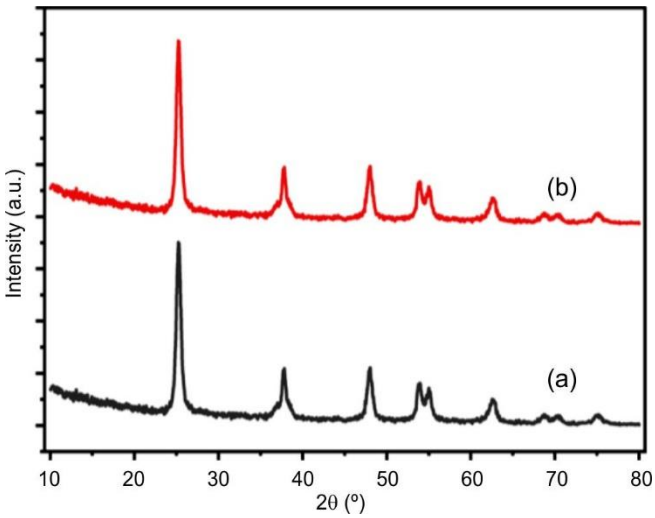

Fig. 13. X-ray diffraction patterns of Ag doped TiO_2 (AgT) (a) before and (b) after the reaction

To study the foremost active species in photocatalytic degradation of AAVN dye using AgT, BiT, NiT and bare TiO_2, by the addition of free radical scavengers' experiments were examined. Effect of free radical scavengers such as isopropyl alcohol (IPA) for hydroxy radicals ($^{\bullet}OH$), ammonium oxalate (AO) and formic acid (FA) as hole scavengers (h^+) and *p*-benzoquinone (*p*-BQ) for superoxide radicals ($^{\bullet}O_2^-$). The photocatalytic activity decreased with *p*-BQ > AO > IPA > no scavenger was observed in Fig. 14. Only 54%, 51%, 53% and 55% of the AAVN was degraded after 180 min when AgT, BiT, NiT and bare TiO_2 were added to dye solution, respectively with *p*-benzoquinone when compared to 98%, 97%, 77% and 95% of the AAVN with Ag-doped TiO_2 in the absence of scavengers. Degradation of AAVN dye was slightly suppressed with the addition of ammonium oxalate *i.e.*, 93% dye was removed in 180 min of when Ag-doped TiO_2 was added to dye solution. The results indicate that a large number of hydroxyl radicals were generated when AAVN dye was irradiated under visible light. Also, the suppression of activity is greater in presence of BQ indicating the dominant role played by superoxide radicals in the mechanism. This suggests that though as XPS studies Bi^{3+} seem to have higher electronegativity difference with Ti^{4+} that can result in high oxidation reactivity on account of generation of greater number of $OH^{-\bullet}$ radicals, the simultaneous reduction process by photogenerated electrons leading to the formation of superoxide radicals which further are responsible for the degradation of the dye/organic pollutant seems to dominate. Hence, Ag- doped catalyst seems to be superior in degrading the pollutants both in presence of visible as well as sunlight.

The degradation of AAVN dye was examined by total organic carbon (TOC) determination. A solution of 100 ppm AAVN dye was prepared with 75 mg bare TiO_2 and AgT nanocatalysts used for determining TOC and the result showed 92% and 96% of TOC is removed by mineralisation.

The photo-degradation mechanism (**Scheme-I**) involves generation of electron-hole pairs on irradiation of doped TiO_2 photocatalyst as the first step. Doping TiO_2 with Ag leads to a reduction in band gap energy, thereby enhancing light absorption in the visible region and facilitating more efficient

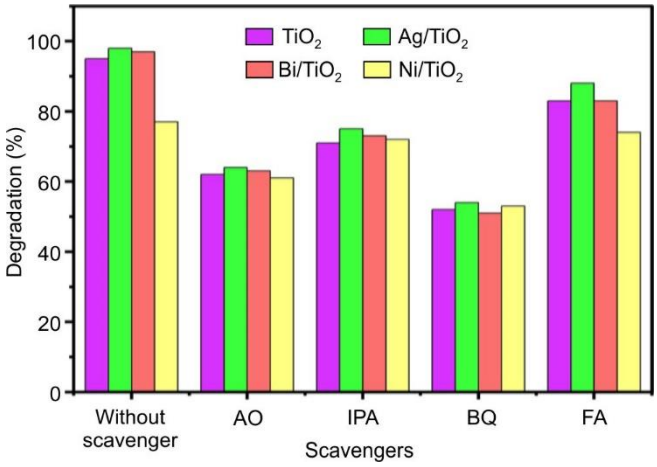

Fig. 14. Scavenger studies data of TiO_2, AgT, NiT and BiT nanocatalysts

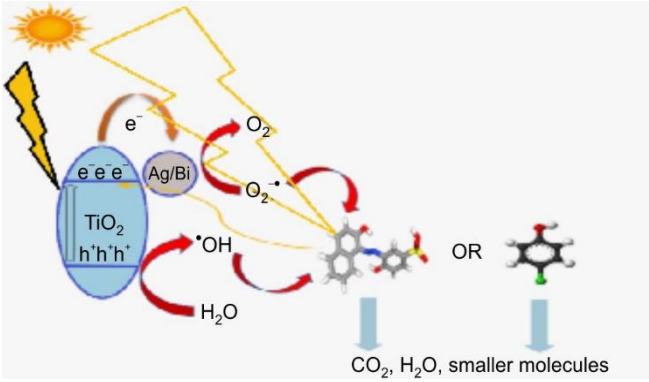

Scheme-I: Probable scheme of the photocatalytic degradation mechanism

charge transfer processes. The presence of Ag also promotes electron trapping, which suppresses the recombination of photogenerated electron-hole pairs and enhances the generation of reactive oxygen species. In this process, photogenerated electrons in the conduction band of TiO_2 are transferred to adsorbed oxygen molecules or dissolved oxygen, resulting in the formation of superoxide radicals ($O_2^{\bullet-}$). Simultaneously, photogenerated holes in the valence band interact with the surface-adsorbed water molecules or hydroxyl ions to generate hydroxyl radicals ($OH^{\bullet-}$). These highly reactive radical species subsequently participate in the oxidative degradation of AAVN dye and 4-chlorophenol, ultimately breaking them down into smaller, less harmful molecules.

Conclusion

Metal-ion doped nano-TiO_2 catalysts were synthesised by simple sol-gel method and explored for the photocatalytic degradation of acid alizarin violet N (AAVN) dye and 4-chlorophenol (4-CP) in presence of visible and sunlight. The characterisation of the parent TiO_2 and doped-TiO_2 nanoparticles revealed only the anatase phase from XRD patterns indicating the successful doping of metal ions into the TiO_2 crystal structure. The nanosize of these catalysts was confirmed from XRD, SEM and TEM analyses. Further, the spherical morphology with minimum agglomeration of particles could be established from SEM and TEM results. The doping of metal ions resulted in the decrease in particle size which is also confirmed from the enhanced BET-specific surface areas of the doped catalysts in comparison to the bare TiO_2. Metal ion doping reduced the band gap of the catalysts as measured from the UV-DRS plots. Also, the doping has resulted in the shift of the emission peak of TiO_2 and reduction of electron-hole recombination rate as evidenced from the PL studies. XRD and EDAX reveal the presence of Ti, Ag, Ni, Bi, C and O in the doped catalysts while XPS analyses discloses the surface chemical states of elements (Ti^{4+}, Ag^{+}, Ni^{2+}, Bi^{3+}, O^{2-}/OH^{-} and C) in doped-TiO_2 and bare TiO_2. The metal ion doped-nano TiO_2 exhibited higher degradation performance of AAVN dye and 4-CP in presence of both visible as well as sunlight over the parent TiO_2 catalyst. AgT showed higher photocatalytic degradation rate among all other metal-doped and undoped TiO_2 catalysts. AgT nanocatalyst was stable and reusable without any appreciable loss of catalytic activity up to the five runs. The degradation was found to higher *i.e.*, 98% at 100 ppm of AAVN dye solution with 75 mg AgT catalyst and 97% of 50 ppm of 4-chlorophenol under visible light irradiation. The lowering of particle size, reduced band gap of TiO_2 and decreased electron-hole recombination rate from the characterisation results correlate well with the enhanced photocatalytic degradation rate of AAVN dye and 4-CP over metal ion doped-TiO_2 especially AgT catalyst.

ACKNOWLEDGEMENTS

The authors acknowledge OU-DST-PURSE-II and OU-UGC-SAP DRS-II for financial support toward the procurement of chemicals. The authors express their sincere gratitude to Prof. M. Vithal, Emeritus Scientist, Department of Chemistry, Osmania University, Hyderabad, for generously providing access to the laboratory facilities and instrumentation. The authors also thank Dr. A. Venugopal and Dr. N. Lingaiah, Chief Scientists at CSIR-IICT, Hyderabad, India for their valuable support in the catalyst characterization.

CONFLICT OF INTEREST

The authors declare that there is no conflict of interests regarding the publication of this article.

DECLARATION OF AI-ASSISTED TECHNOLOGIES

During the preparation of this manuscript, the authors used an AI-assisted tool(s) to improve the language. The authors reviewed and edited the content and take full responsibility for the published work.

REFERENCES

1. S. Benkhaya, S. M'rabet and A. El Harfi, *Inorg. Chem. Commun.*, **115**, 107891 (2020); https://doi.org/10.1016/j.inoche.2020.107891
2. L. Nambela, L. V. Haule, and Q. Mgani, *J. Clean. Prod.*, 246, 119036 (2020); https://doi.org/10.1016/j.jclepro.2019.119036
3. M.Y. Ghadhban, H.S. Majdi, K.T. Rashid, Q.F. Alsalhy, D.S. Lakshmi, I.K. Salih and A. Figoli, *Membranes*, **10**, 47 (2020); https://doi.org/10.3390/membranes10030047
4. G.K. Fobiri, *Textile Leather Rev.*, **5**, 180 (2022); https://doi.org/10.31881/TLR.2022.22

5. J. Fischbach, Q. Loh, F.F. Bier, T.S. Lim, M. Frohme and J. Glökler, *Sci. Rep.*, **7**, 45085 (2017); https://doi.org/10.1038/srep45085
6. R. Al-Tohamy, S.S. Ali, F. Li, K.M. Okasha, Y.A.-G. Mahmoud, T. Elsamahy, H. Jiao, Y. Fu and J. Sun, *Ecotoxicol. Environ. Safety*, **231**, 113160 (2022); https://doi.org/10.1016/j.ecoenv.2021.113160
7. R. Kishor, D. Purchase, G.D. Saratale, R.G. Saratale, L.F.R. Ferreira, M. Bilal, R. Chandra and R.N. Bharagava, *J. Environ. Chem. Eng.*, **9**, 105012 (2021); https://doi.org/10.1016/j.jece.2020.105012
8. I. Ullah, A. Haider, N. Khalid, S. Ali, S. Ahmed, Y. Khan, N. Ahmed and M. Zubair, *Spectrochim. Acta A Mol. Biomol. Spectrosc.*, **204**, 150 (2018); https://doi.org/10.1016/j.saa.2018.06.046
9. J. Huang, H. Song, C. Chen, Y. Yang, N. Xu, X. Ji, C. Li and J.A. You, *J. Environ. Chem. Eng.*, **5**, 2579 (2017); https://doi.org/10.1016/j.jece.2017.05.012
10. S. Naseem, W. Khan, S. Khan, I. Uddin, W. Raza, M. Shoeb, M. Mobin and A.H. Naqvi, *J. Electron. Mater.*, **48**, 7203 (2019); https://doi.org/10.1007/s11664-019-07499-7
11. M.A. Majeed Khan, R. Siwach, S. Kumar and A.N. Alhazaa, *Opt. Laser Technol.*, **118**, 170 (2019); https://doi.org/10.1016/j.optlastec.2019.05.012
12. T. Raguram and K.S. Rajni, *Appl. Phys., A Mater. Sci. Process.*, **125**, 288 (2019); https://doi.org/10.1007/s00339-019-2581-1
13. J. Xu, Y. Ao, D. Fu and C. Yuan, *Appl. Surf. Sci.*, **255**, 2365 (2008); https://doi.org/10.1016/j.apsusc.2008.07.095
14. C. Wattanawikkam and W. Pecharapa, *Radiat. Phys. Chem.*, **171**, 108714 (2020); https://doi.org/10.1016/j.radphyschem.2020.108714
15. V. Moradi, M.B. Jun, A. Blackburn and R.A. Herring, *Appl. Surf. Sci.*, **427**, 791 (2018); https://doi.org/10.1016/j.apsusc.2017.09.017
16. X. Zhu, H. Xu, Y. Yao, H. Liu, J. Wang, Y. Pu, W. Feng and S. Chen, *RSC Adv.*, **9**, 40003 (2019); https://doi.org/10.1039/C9RA08655B
17. A. Sirivallop, T. Areerob, and S. Chiarakorn, *Catalysts*, **10**, 251 (2020); https://doi.org/10.3390/catal10020251
18. A. Khlyustova, N. Sirotkin, T. Kusova, A. Kraev, V. Titova and A. Agafonova, *Mater. Adv.*, **1**, 1193 (2020); https://doi.org/10.1039/D0MA00171F
19. M. Kunnamareddy, R. Rajendran, M. Sivagnanam, R. Rajendran and B. Diravidamani, *J. Inorg. Organomet. Polym. Mater.*, **31**, 2615 (2021); https://doi.org/10.1007/s10904-021-01914-5
20. M.M. Haque, A. Khan, K. Umar, N.A. Mir, M. Muneer, T. Harada and M. Matsumura, *Energy Environ Focus*, **2**, 73 (2013); https://doi.org/10.1166/eef.2013.1029
21. A.K. Gupta, P. Srivastava and L. Bahadur, *J. Appl. Phys.*, **122**, 724 (2016); https://doi.org/10.1007/s00339-016-0241-2
22. B. Rajamannan, S. Mugundan, G. Viruthagiri, P. Praveen and N. Shanmugam, *Int. J. Curr. Res.*, **5**, 2863 (2013); https://doi.org/10.1016/j.saa.2013.09.045
23. B.-G. Park, *Gels*, **8**, 14 (2021); https://doi.org/10.3390/gels8010014
24. X.F. Lei, X.X. Xue and H. Yang, *Appl. Surf. Sci.*, **321**, 396 (2014); https://doi.org/10.1016/j.apsusc.2014.10.045
25. F.B. Li and X.Z. Li, *Chemosphere*, **48**, 1103 (2002); https://doi.org/10.1016/S0045-6535(02)00201-1
26. L. Sun, J. Zhai, H. Li, Y. Zhao, H. Yang and H. Yu, *ChemCatChem*, **6**, 339 (2014); https://doi.org/10.1002/cctc.201300879
27. C. Ma, X. Wang, H. Luo and D. Zhang, *J. Mater. Sci. Mater. Electron.*, **28**, 10715 (2017); https://doi.org/10.1007/s10854-017-6847-0
28. K.S. Kim and R.E. Davis, *J Electron Spectrosc. Rel. Phenomena*, **1**, 251 (1972); https://doi.org/10.1016/0368-2048(72)85014-X